

The key role of aromaticity in the structure and reactivity of C₆₀ and endohedral metallofullerenes

Marc Garcia-Borràs^{a,b*}, Josep M. Luis^b, Miquel Solà^{b*} and Sílvia Osuna^{b*}

^a *Department of Chemistry and Biochemistry, University of California, Los Angeles, California 90095, United States.*

^b *Institut de Química Computacional i Catàlisi (IQCC) and Departament de Química, Universitat de Girona, c/ Maria Aurèlia Capmany 6, 17003 Girona, Catalonia, Spain. E-mail: miquel.sola@udg.edu, silvia.osuna@udg.edu.*

Abstract

In this review, we show that the local aromaticity of C₆₀ and endohedral metallofullerenes (EMFs) is a key factor to understand and predict their structure and reactivity. We report recent examples provided by our group that highlight the importance of aromaticity in C₆₀ and EMFs. First example discusses the regioselectivity of Diels-Alder reactions in reduced C₆₀; the second one analyzes how aromaticity stabilizes the most suitable hosting cages in EMFs; the third one determines the effect of aromaticity in the relative abundances of EMFs; the fourth one shows a relationship between aromaticity and the stability of EMF adducts formed in Bingel-Hirsch (BH) reactions; and the last one proposes structural criteria to predict the regioselectivity in BH reactions based on the local aromaticity of EMFs.

Introduction

The striking discovery of the fullerenes was made in 1985 by Kroto, Curl and Smalley, when trying to simulate the conditions of cool red giant stars in the laboratory. They obtained a 720 mass peak (i.e. C₆₀), which appeared to be extremely strong [1]. In fact, C₆₀ was observed five years before by Iijima in vacuum-deposited amorphous carbon films containing carbon nano-onions, although Iijima did not realize the presence of C₆₀ in the films until 1987 [2, 3]. The new molecule discovered was named buckminsterfullerene as homage to the geodesic dome architect, Buckminster Fuller, and was later confirmed using single-crystal X-ray diffraction (XRD) [4]. Since their discovery, many fullerene structures have been synthesized and a variety of studies regarding the fullerene stability, characterization, properties such as aromaticity, and reactivity have been reported [5-13].

Fullerenes are polyhedral with carbon atoms placed at the vertices, bonds in edges, and rings in faces. As a general rule, fullerenes contain 12 pentagonal rings and a variable number of hexagonal rings ($k/2-10$, where k is the number of atoms). Nevertheless, fullerenes containing 4 and 7 membered rings have been reported recently [14, 15]. Many isomers can be obtained for a fix number of atoms, and rules to elucidate which isomers are more stable are needed. In this line, Kroto proposed the Isolated Pentagon Rule (IPR), which identifies the most stable fullerene isomers as those that dispose the 12 pentagons totally isolated [16]. Having two pentagonal rings fused produces a pentalene unit, which according to the 4N Hückel rule has a destabilizing effect over the π electronic structure. The IPR has been extensively used especially for free fullerene structures, as it reduces quite dramatically the number of possible isomers for a given fullerene.

Right after the C₆₀ discovery, the possibility of incarcerating atoms or clusters inside the fullerene cage was postulated. Indeed, La@C₆₀ was detected the same year of the discovery [17]. It took some years, however, to achieve the formation of lanthanum-based metallofullerenes (La@C_k, $k= 70, 74, 82$) in macroscopic quantities [18]. These new structures were named endohedral fullerenes (EFs) or endohedral metallofullerenes (EMFs) in the most common case of having metal-based clusters encapsulated. Shinohara and coworkers characterized by X-ray the first EMF in 1995 [19]. Since then, many other EMFs have been reported which includes the so-called classical, metallic carbides, metallic tri-nitride template

(TNT), metallic oxides and sulfides [20, 21]. The most abundant fullerene structure after C_{60} and C_{70} was reported in 1999 by Balch and co-workers, i.e. $Sc_3N@I_h-C_{80}$, which is the first member of the TNT family [22]. The charge distribution in these $X_3N@C_k$ EMFs can be formally described as $(X_3N)^{6+}@C_k^{6-}$, although the real charge transferred is always lower as covalent interactions between the TNT and the fullerene are rather strong [23]. Depending on the nature of the encapsulated cluster, the formal charge transferred to the fullerene cage may be lower [24]. Poblet and coworkers proposed the (LUMO+3)-(LUMO+4) rule to identify which structures could be good candidates for encapsulating TNT units: those empty fullerene cages presenting a large (LUMO+3)-(LUMO+4) gap might form TNT-based EMFs [25-27]. In line with this simple ionic model, Popov and Dunsch [28] also observed that the relative stabilities of $M_3N^{6+}@C_k^{6-}$ ($k = 68-98$) correlate well with those of their corresponding empty charged cages (C_k^{6-}). The negative charge in the latter structures is not evenly distributed and it accumulates in five-membered rings (5-MRs) [29, 30]. The reason is that anionic cyclopentadiene and pentalene are aromatic (unlike their neutral forms), and thus they better stabilize the excess of electrons. The IPR rule is usually more a suggestion than a rule in these EMF structures, and additional criteria are needed to rationalize the EMF preferences. Alcamí and coworkers found that in these charged cages, the most stable isomers present a well-separated negatively charged adjacent pentagon pairs (APPs) and positively charged pyrene motifs [30]. This was further investigated and confirmed by Poblet *et al.* that defined the so-called inverse pentagon separation index (IPSI) to quantify the pentagon separation [29]. As we will show in this review, aromaticity plays also a key role in determining the most stable isomer for the EMF encapsulation [31]. Aromaticity can also be used to rationalize the experimental EMF abundances obtained in the laboratory [32].

The formal charge transfer that takes place on EMFs [25] has severe consequences on the reactivity [31, 33, 34], aromaticity [32, 35, 36], and relative stabilities [28] of these compounds. Empty fullerenes generally react with those bonds situated between hexagons (i.e. called [6,6]), whereas EMFs and negatively charged C_{60} often prefer [5,6] bonds [31, 37]. Since their discovery, fullerenes but in particular EMFs have engendered a huge interest due to their potential application in a variety of fields [38, 39]. Of interest is their exohedral functionalization as it allows the bio-application of these compounds as they usually exhibit low solubility in water, but also to tune their properties for designing new materials and nano-devices. The chemical functionalization is generally achieved *via* cycloaddition reactions such as Diels-Alder (DA), 1,3-dipolar, and nucleophilic [2+1] Bingel-Hirsch (BH) additions. Many efforts have been devoted to explore the exohedral reactivity of several EMFs. For a complete review check references [34, 40]. The first exohedral functionalization of an EMF was the DA cycloaddition of 6,7-dimethoxy-isochroman-3-one to the archetypal $Sc_3N@I_h-C_{80}$ [41]. DFT calculations confirmed that the [5,6] addition was at least 11 kcal/mol more favorable than the [6,6] [37, 42, 43]. The Prato reaction of $M_3N@I_h-C_{80}$ was also achieved [44] and it was found that the regioselectivity of the process is highly dependent on the nature of the encapsulated cluster [44-48]. On the other hand, the BH addition to $M_3N@I_h-C_{80}$ ($M = Sc, Lu, Y, \text{ and } Er$) occurs regioselectively on the [6,6] bond [49]. These representative studies highlight the huge effect exerted by the encapsulated clusters in directing the fullerene addition sites.

Computational studies have been key to rationalize, predict, give support, and even correct some experimental assignments [33, 34, 50-52]. The functionalization preferences have been rationalized using bond distances together with pyramidalization angles, properly shaped LUMO orbitals to react with the diene, and more recently fullerene distortion energies and aromaticity measures [31, 33, 34, 53]. In this article, we review our most recent aromaticity-based studies involving fullerenes, and endohedral metallofullerenes (EMFs). This review highlights different aspects of the aromaticity of fullerenes and EMFs, and puts a special focus on how aromaticity can be used to rationalize, but most importantly, to predict their molecular structure and reactivity.

1. Electrochemical control of the regioselectivity in the exohedral functionalization of C₆₀: the role of aromaticity

The Diels-Alder (DA) cycloaddition involving C₆₀ has been extensively studied, and it is well known that both the kinetic and thermodynamic addition takes place regioselectively on the pyracylenic [6,6] bond [54, 55]. We computed the complete reaction path for the DA reaction between cyclopentadiene (Cp) and C₆₀ on [6,6] and [5,6] positions, as showed in Figure 1, finding that the [6,6] reaction barrier and reaction energy are *ca.* 12 and 16 kcal/mol more favorable than those for the [5,6] addition [56]. Nevertheless, our calculations revealed that when C₆₀ fullerene is reduced with up to 6 electrons, the tendency is inverted becoming the addition on [5,6] position the most favored from kinetic and thermodynamic points of view. The differences in the reaction energies and barriers for the additions on [6,6] and [5,6] bonds when adding $n=0-6$ electrons to the fullerene are represented in Figure 1. Negative differences indicate that the addition on [6,6] bond is favored while positive differences indicate a more favorable addition on [5,6] position. Thermodynamic and kinetic behaviors are found to follow the same trend. Thus, the regioselectivity of the DA addition on C₆₀ can be controlled by electrochemical reduction of the fullerene molecule.

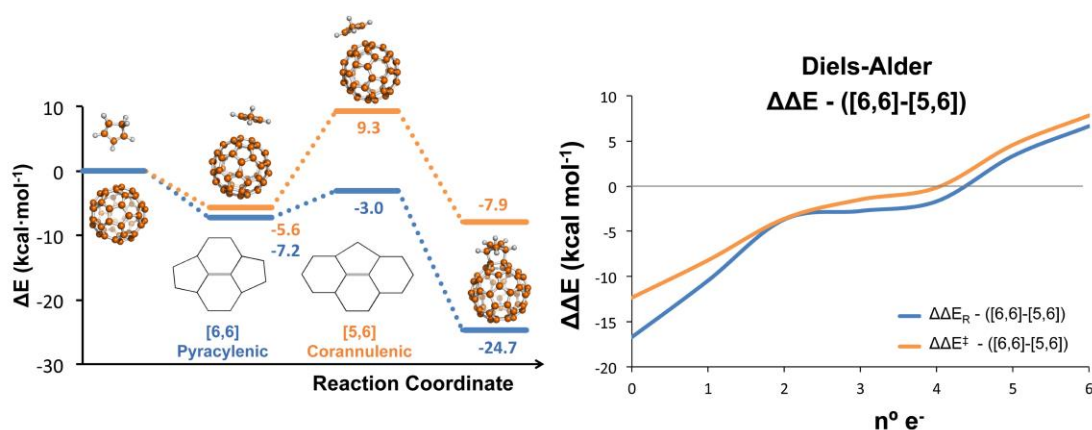


Figure 1. Electronic energy profiles obtained at BP86-D2/TZP//BP86-D2/DZP level of the Diels-Alder addition of cyclopentadiene to the [5,6] and [6,6] bonds of C₆₀ (left); and energy differences in reaction energies (ΔE_R) and reaction barriers (ΔE^\ddagger) for the additions on [6,6] and [5,6] bonds when the C₆₀ is reduced by n electrons ($n=0-6$). Energies are given in kcal/mol. Reproduced from ref. [56] with permission from The Royal Society of Chemistry.

In order to analyze this change on the DA regioselectivity, we studied the changes in the aromaticity of the five- and six-membered rings (5-MRs and 6-MRs) [57-61]. As showed in Figure 2, we found that aromaticity of 5-MRs increases while the 6-MRs decreases when electrons are added to the C₆₀ molecule. It has been shown that charge distribution in anionic fullerenes is not uniform, and the negative charge is mainly localized on 5-MRs [29]. As a consequence, when a 5-MR is negatively charged, it becomes more cyclopentadienyl anion-like, which fulfills the Hückel $4N+2$ rule, and thus becomes more aromatic. On the contrary, the negative charge induces a decrease of the 6-MR aromaticity because they lose the ideal $4N+2$ electronic structure.

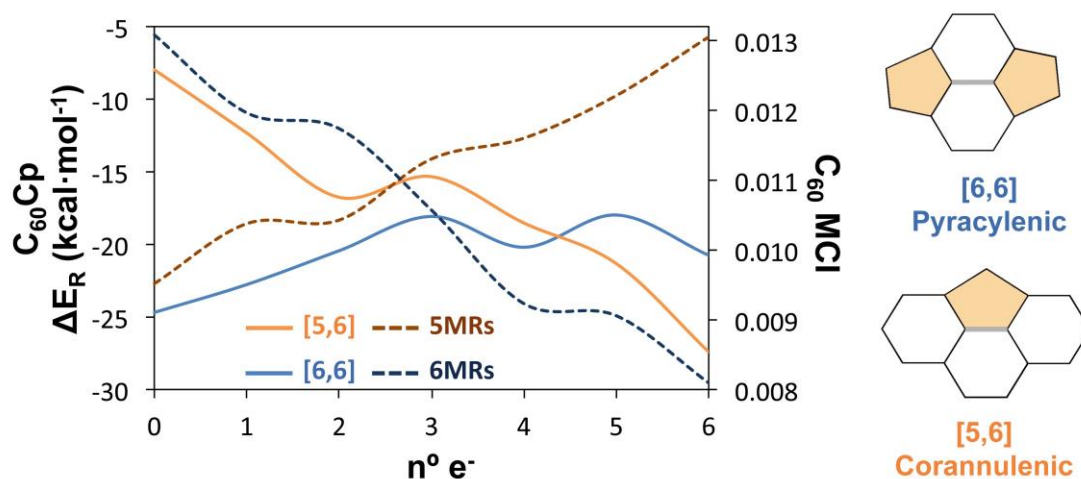


Figure 2. Representation of the reaction energies (ΔE_R , kcal/mol, solid lines) for the Diels-Alder reaction of cyclopentadiene to [6,6] and [5,6] bonds of C_{60} and aromaticity multicenter electronic index (MCI) values (dashed lines, in electrons) of the 5-MRs and 6-MRs in C_{60} when the fullerene is reduced by n electrons. Reproduced from ref. [56] with permission from The Royal Society of Chemistry.

When the reaction takes place on a pyraclyenic [6,6] bond type, the π conjugation of two 5-MRs and two 6-MRs is lost. On the other hand, when the addition is on a corannulenic [5,6] bond, the conjugation vanishes in three 6-MRs and one 5-MR. From this observation, we can rationalize the changes induced in the regioselectivity of the reaction. A higher aromaticity of a given ring implies more resistance towards an attack over one of its bonds, and *vice versa* for lower aromaticity. Consequently, for neutral C_{60} , the [6,6] addition is preferred because it involves the removal of the conjugation in only two 6-MRs (the most aromatic) as compared to the [5,6] addition that affects three 6-MRs. On the other hand, when 6 electrons are transferred to the C_{60} , the 5-MRs are the most aromatic and the [5,6] addition barrier is lower in energy because it only destroys the conjugation of one aromatic 5-MR.

We have shown that it is possible to electrochemically control the regioselectivity in the DA reaction on fullerenes. The change in regioselectivity upon reduction can be rationalized in terms of the local aromaticity of the 5- and 6-MRs. Negatively charged fullerenes are used as models for describing the structure of EMFs. In that sense, our results could help in explaining why in EMFs the DA on [6,6] position is not regioselectively preferred and [5,6] adducts are often obtained, in contrast to what happens for empty and neutral fullerenes.

2. Maximum aromaticity as a guiding principle to determine most suitable hosting cages in endohedral metallofullerenes

In our previous work, we found that when negative charge is transferred to a fullerene cage the aromaticity of its 5-MRs and 6-MRs is modified. In addition, it was previously reported that there exists a correlation between the negative charge centered on 5-MRs and the relative stability of C_{2n} anionic fullerenes with the same number of carbons and adjacent pentagon pairs (APPs) [27, 29]. Anionic fullerene isomeric structures are good models for describing EMF stabilities [28], as their electronic structure can be described using the ionic model (for example, $M_3N^{6+}@C_{2n}^{6-}$ for TNTs, or $M_2C_2^{4+}@C_{2n}^{4-}$ for metallic carbides).

Based on the mentioned precedents, we suggested that the aromaticity of the fullerene rings could have also a key role on the stability of endohedral metallofullerene structures [31]. In this line, we proposed the additive local aromaticity (ALA) index as an aromaticity indicator

for the study of the stability of negatively charged fullerene isomers. ALA index is defined as the sum of the local aromaticities of all rings in the cage:

$$ALA = \sum_{i=1}^n A_i$$

where A_i is the local aromaticity of ring i , and n is the number of rings in the fullerene, including both 5- and 6-MRs. This index aims to be a representative indicator for comparing the local aromaticities of the rings in different fullerene cages with the same number of carbon atoms.

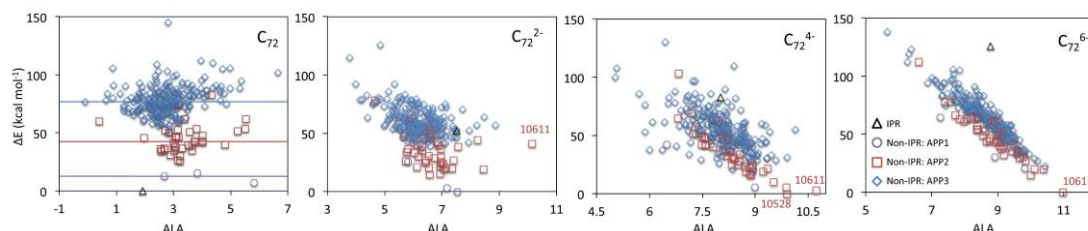


Figure 3. Relative stabilities (at AM1 level) of C_{72}^{m-} isomers with 1-3 APPs with respect to the ALA index. The lines in C_{72} neutral case indicate the relative average energies with respect to the energy of the IPR isomer for each isomeric type. Isomers experimentally observed in EMFs are indicated with their corresponding label. Reprinted with permission from ref. [31].

We have computed the ALA index using the geometric HOMA aromaticity indicator [62, 63] for all the possible C_{72} isomers with 0, 1, 2, and 3 APPs and we have compared them with their relative stabilities computed at AM1 level. We used HOMA but, as recently show, aromaticity criteria based on structure, electron delocalization and energy can be unified [64]. As showed in Figure 3, no correlation between the relative stability and aromaticity is found when the neutral fullerene is considered. The most stable isomer is the IPR one, and when the number of APPs increases, the relative stability of the fullerene isomers decreases. The latter was expected from the isolated pentagon rule (IPR) and the pentagon adjacency penalty rule (PAPR) [65]. Nevertheless, when the negative charge of the fullerene isomers increases up to six electrons, we found a very good correlation between the relative stabilities of the fullerene isomers and their local aromaticities in terms of ALA index, regardless of the number of APPs they have. Here it is important to remark that C_{2n} hexaanions are very good models for describing the relative stabilities of endohedral metallofullerenes [26]. The most stable C_{72}^{6-} isomer, the non-IPR (10611)- C_{72} cage, which experimentally forms $La_2^{6+}@C_{72}^{6-}$ EMF, is the one that exhibits the largest ALA index value among all C_{72}^{6-} cage isomers. Thus, our results indicate that the most stable anionic isomers are those that maximize their local aromaticity (Maximum Aromaticity Criterion, MARC). In addition to that, our results explain why the IPR rule is no longer fulfilled when EMFs are considered. The isomer that can better stabilize the negative charge transferred by the encapsulated metal cluster is the most aromatic one, regardless the number of pentagon adjacent pairs it has.

We systematically computed the ΔE vs. ALA for a large amount of all the possible isomers for the most common C_{2n} ($2n=66-104$) EMFs reported to date, including IPR and non-IPR cages in their anionic form. The considered negative charge depends on the formal electron transfer from the metallic cluster to the fullerene. Our results, summarized in Figure 4, indicate that fullerene isomers that are experimentally detected forming EMFs, are those that have the largest local aromaticities in terms of the ALA index. This prediction only partially fails for those EMFs in which the charge transfer is of two electrons (C_{66}^{2-} and C_{94}^{2-}). The reason is that in these cases, the role of aromaticity in the stabilization of the cages is less important than when four or six electrons are transferred.

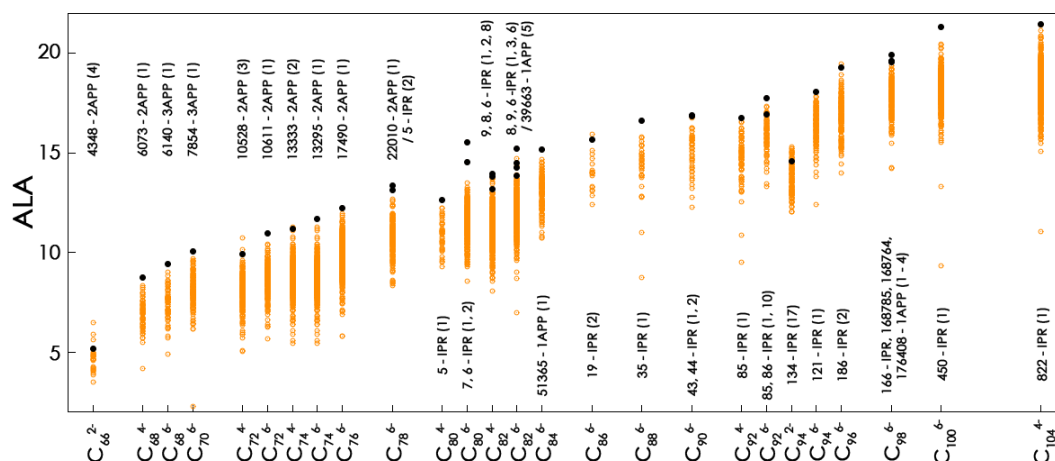


Figure 4. Classification in terms of the ALA index of the anionic IPR and non-IPR fullerene isomers with 1-3 APPs for the most common C_{2n} ($2n=66-104$) EMFs reported to date. Isomers experimentally observed are marked using black dots, and their corresponding isomer labels are indicated. The ALA prediction ordering for the experimentally observed isomers are given in parentheses. Reprinted with permission from ref. [31].

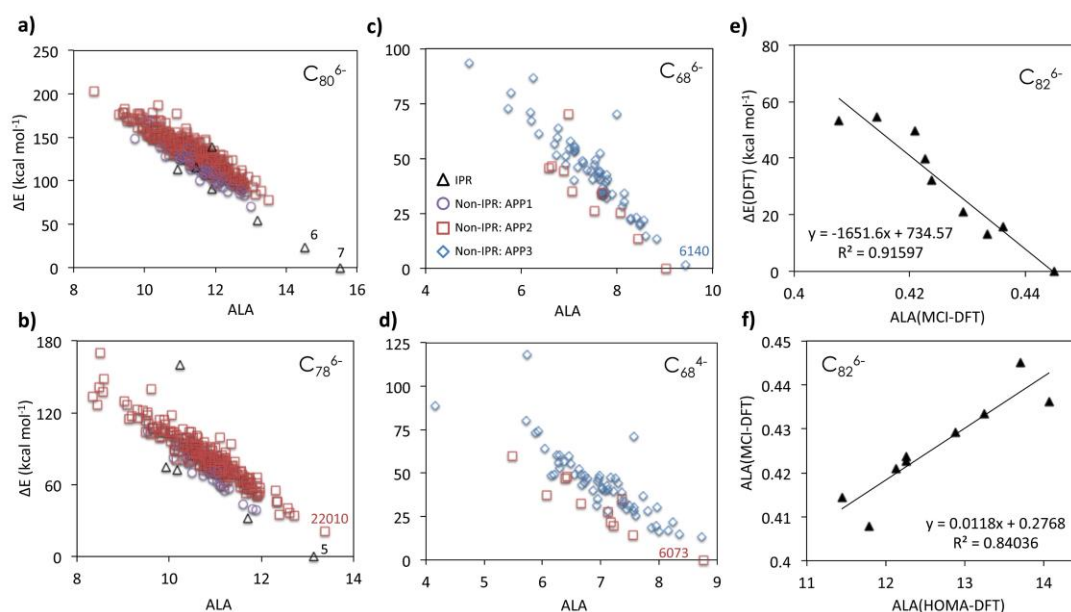


Figure 5. Relative stabilities (at AM1 level) of a) C_{80}^{6-} , b) C_{78}^{6-} , c) C_{68}^{6-} , and d) C_{68}^{4-} isomers with 1-3 APPs with respect to the ALA index. Isomers experimentally observed in EMFs are indicated with their corresponding label. e) Relative stabilities (at BP86/DZP level) of C_{82}^{6-} IPR isomers versus the computed ALA index using MCI measures. f) Computed ALA index using MCI index for C_{82}^{6-} IPR isomers versus computed ALA index using HOMA index. Reprinted with permission from ref. [31].

The proposed maximum aromaticity criterion can predict the formation of a non-IPR EMF, as for instance the case of C_{72}^{6-} . But it can also predict the stabilization of an IPR EMF isomer. For example, C_{80} -based TNT EMFs can be synthesized in two different IPR isomeric forms: the I_h - C_{80} ($Sc_3N@I_h$ - C_{80} , the most abundant EMF), and D_{5h} - C_{80} ($Sc_3N@D_{5h}$ - C_{80} , less abundant). These two isomers are the C_{80}^{6-} isomers with the largest ALA values, as showed in Figures 4 and 5a. The same good performance of the aromaticity criterion and ALA index is

found to describe mixed IPR and non-IPR EMFs formation, as for example in C_{78}^{6-} systems (see Figure 5b).

Depending on the nature of the metallic cluster encapsulated, different number of electrons are formally transferred from the cluster to the fullerene. Our results also showed that using the ALA index one can rationalize the different isomer stabilization when six (Figure 5c) or four electrons (Figure 5d) are transferred, for example, to the C_{68} fullerene.

Finally, we also showed that the maximum aromaticity criterion does not depend on the method used for computing the local aromaticities of the fullerene rings. The same trends and correlations are found when using the electronic multicenter index MCI and DFT optimized structures (see Figure 5e) instead of HOMA aromaticity measures and the AM1 optimized structures (see Figure 5f).

3. Understanding the relative abundances of TNT-based endohedral metallofullerenes from aromaticity measures

Following the line started with our previous study, we generalized the ALA index to expand its scope [32]. In this work, we proposed the normalization of the ALA index per number of rings present in the fullerene structure to allow the comparison between fullerenes with different number of carbon atoms, as follows:

$$ALAN = \frac{1}{n} \sum_{i=1}^n A_i$$

where A_i is the local aromaticity of ring i , and n is the number of rings in the fullerene, including both 5- and 6-MRs. In order to compare $ALAN$ measures, which include different number of rings, we needed to use an accurate aromaticity index, which equally treats both ring types. In that sense, we proposed to use the normalized version of the MCI multicenter index, the so-called I_{NB} electronic index [57-61].

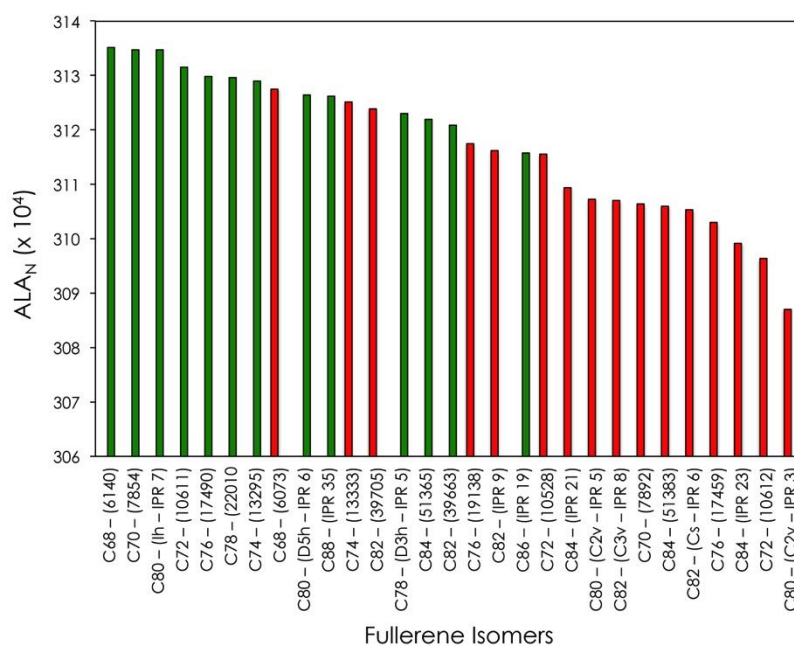


Figure 6. Classification in terms of the $ALAN$ index (calculated at B3LYP/6-31G//BP86/DZP level) of the hexaanionic most stable C_{2n} isomers, which also exhibit the largest ALA values for each C_{2n} ($2n=68-88$) fullerene family, obtained from our previous work [31]. Isomers

experimentally observed containing TNT units are displayed in green, while isomers experimentally not formed are colored in red. Aromaticity results are given as $ALA_N \times 10^4$ values. Reproduced from ref. [32] with permission from The Royal Society of Chemistry.

In Figure 6, we summarize the ALA_N values for selected C_{2n} ($2n=68-88$) isomers, sorted by their ALA_N values. As a general trend, fullerene isomers experimentally observed containing TNT moieties have the largest ALA_N values, which indicates that they are more aromatic in terms of ALA_N . The rest of thousands less stable C_{2n} isomers exhibit lower ALA_N values (lower ALA values, from our previous work). Thus, our computations indicate that the most aromatic C_{2n} ($2n=68-88$) fullerene cages, independently of their size or their number of APPs, are those most suitable for stabilizing a TNT-based EMF.

Finally, we applied the ALA_N index for the analysis of the relative abundances of $Sc_3N@C_{2n}$ ($2n=68-88$) EMFs. We have computed the aromaticity in terms of ALA_N using the electronic delocalization I_{NB} index for the optimized EMFs structures explicitly containing scandium TNT metallic cluster inside. The results, summarized in Figure 7, demonstrate that the most abundant EMF, $Sc_3N@I_h-C_{80}$, is by far the most aromatic scandium-based TNT EMF. The second most aromatic EMF is $D_{5h}-C_{80}$, followed by the $Sc_3N@C_{68}$ and $Sc_3N@C_{78}$ TNTs, which are the following most abundant scandium based TNT EMFs obtained from a common arc discharge synthesis. Consequently, our results indicate that the ALA_N index obtained for Sc_3N based EMFs can be used to predict the abundances of EMFs regardless the fullerene cage size or the number of adjacent pentagon pairs, being the experimentally detected most abundant EMFs formed the most aromatic ones.

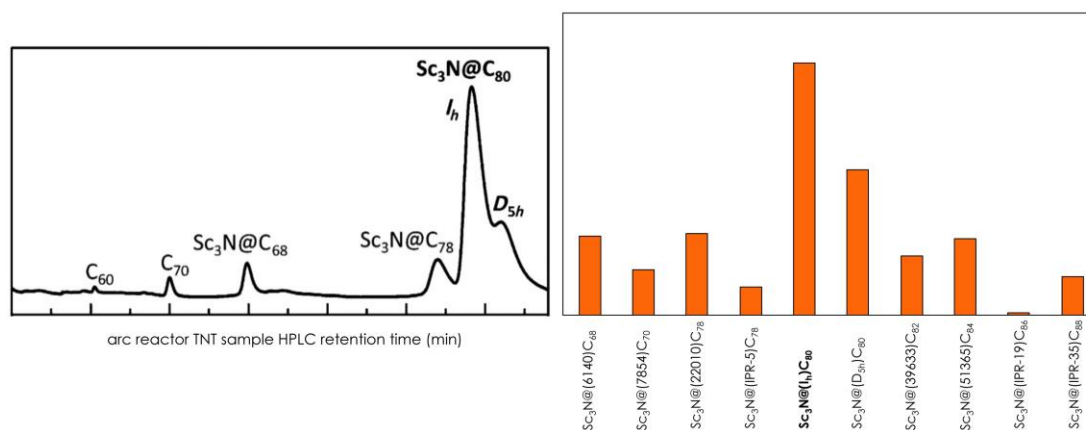


Figure 7. Right: Relative ALA_N values (calculated at B3LYP/6-31G//BP86/DZP level) for $Sc_3N@C_{2n}$ fullerenes, sorted by increasing cage size; Left: Quantitative HPLC chromatograms of the arc reactor carbon sample of a typical scandium based TNT EMFs synthesis (from Prof. Echegoyen lab, ref [66]). Reproduced from ref. [32] with permission from The Royal Society of Chemistry.

4. Aromaticity as the driving force for the stability of non-IPR endohedral metallofullerene Bingel-Hirsch adducts

Bingel-Hirsch (BH) reaction is one of the most employed strategies for functionalizing fullerenes and endohedral metallofullerenes. In general, the thermodynamically most stable EMF products obtained are those corresponding to open-cage adducts (termed fulleroids). None of the traditional parameters used to understand the regioselectivity in EMFs, that is C–C bond distances and pyramidalization angles, are able to describe the stability tendencies found in EMF BH adducts. Based on our previous findings where we relate the endohedral

metallofullerenes stabilities with the local aromaticity of their rings, we have studied the relationship between the aromaticity of the BH EMF monoadducts and their relative stabilities.

We computed the relative stabilities of selected monoadducts, at BP86-D2/TZP//BP86-D2/DZP level, for $\text{Gd}_3\text{N}@C_5(51365)\text{-C}_{84}$, $\text{Y}_3\text{N}@C_2(22010)\text{-C}_{78}$, and $\text{Sc}_3\text{N}@D_3(6140)\text{-C}_{68}$ EMFs, as showed in Figure 8 [36]. In addition, we calculated the ALA index at HOMA level for each optimized BH monoadduct structure. The correlations found between the relative stabilities of the different monoadducts and their corresponding ALA values indicate that the products lowest in energy are those that are more aromatic in terms of local ALA index, independently of the number of APP units on the structure (1 for C_{84} , 2 for C_{78} , and 3 for C_{68} based EMFs).

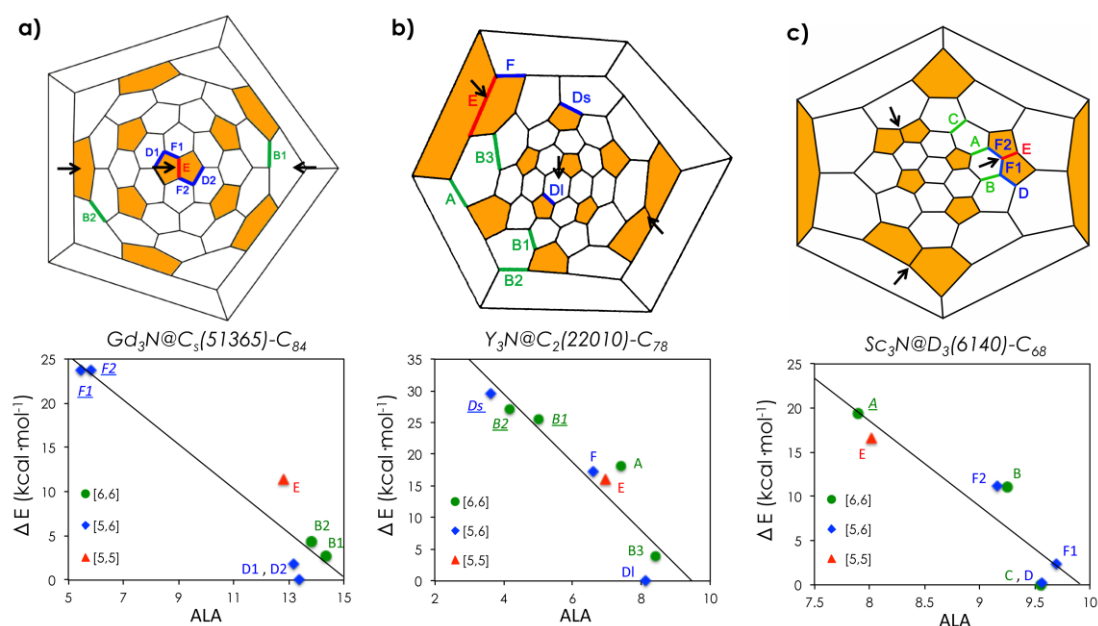


Figure 8. Schlegel diagram representations with the considered bonds and the relative stability of Bingel-Hirsch monoadducts at BP86-D2/TZP//BP86-D2/DZP level with respect to the ALA index of: a) $\text{Gd}_3\text{N}@C_5(51365)\text{-C}_{84}$, b) $\text{Y}_3\text{N}@C_2(22010)\text{-C}_{78}$, and c) $\text{Sc}_3\text{N}@D_3(6140)\text{-C}_{68}$ EMFs. Green circles, blue diamonds, and red triangles represent [6,6], [5,6], and [5,5] bonds, respectively. Closed-cage products are labeled in italics and underlined. The positions of metallic atoms are represented with black arrows and 5-MRs are highlighted in orange. Reproduced from ref. [36] with permission from The Royal Society of Chemistry.

We found that, in general, closed-cage adducts are the least aromatic and the least stable. In these adducts, there is a hybridization change of the attacked carbon atoms from sp^2 to sp^3 , disrupting the π electron delocalization of the rings. On the contrary, in the case of the open-cage structures, all fullerene carbon atoms keep their sp^2 hybridization (large π electron delocalization) resulting in the so-called homofullerenes.

Those products with similar ALA values have similar stabilities, regardless of their bond type. For example, we found that product **C**, a [6,6] monoadduct in $\text{Sc}_3\text{N}@D_3(6140)\text{-C}_{68}$ and product **D**, a [5,6] addition, have relative stabilities of 0.0 and 0.2 kcal/mol, and exhibit equivalent ALA index measures. In addition, aromaticity measures rationalize the different stabilities found for analogous bonds, which have similar C–C bond distances and pyramidalization angles. This is the case, for example, of products **F1** (2.4 kcal/mol) and **F2**

(ca. 11 kcal/mol) in $\text{Sc}_3\text{N}@D_3(6140)\text{-C}_{68}$ EMF that have equivalent bond distances and pyramidalization angles but different ALA measures.

An important observation is that in none of the three studied systems, the thermodynamic addition to the [5,5] bond is favored, as opposite to what is found for the Diels-Alder addition on $\text{Y}_3\text{N}@C_2(22010)\text{-C}_{78}$ EMF [52]. The presence of a metallic atom facing the attacked C-C bond, as experimentally observed in the $\text{Y}_3\text{N}@I_h\text{-C}_{80}$ X-ray monoadduct structures, is also found in most of the optimized most stable products of the studied systems. For example, the latter is observed for the **DI** product of $\text{Y}_3\text{N}@C_2(22010)\text{-C}_{78}$ EMF, as showed in Figure 9. The occupancy of this position by the metal atom, also improves the p-p overlap between the functionalized carbon atom orbitals enhancing the ring π -homoaromaticity.

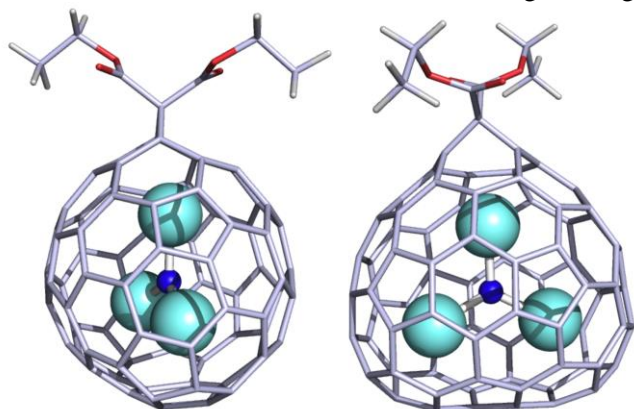


Figure 9. Optimized structure at BP86-D2/DZP of the most stable Bingel-Hirsch $\text{Y}_3\text{N}@C_2(22010)\text{-C}_{78}$ **DI** monoadduct, with an yttrium atom directly facing the functionalized open-cage C-C bond.

Our computational exploration showed that there exists a relationship between the relative stabilities of BH monoadducts of EMFs and their aromaticities measured in terms of ALA index. This fact, confirms that the maximum aromaticity criterion is a powerful tool for analyzing and rationalizing the stability of EMF thermodynamic BH products.

5. Bingel-Hirsch derivatization of TNT endohedral metallofullerenes predicted from simple aromaticity measures. The $\text{Sc}_3\text{N}@D_{3h}\text{-C}_{78}$, and $\text{Sc}_3\text{N}@D_{5h}\text{-C}_{80}$.

As observed in our previous work, we found a relationship between the stability of Bingel-Hirsch EMF monoadducts and their ALA aromaticity [36]. Nevertheless, the group of Prof. Poblet demonstrated that the BH reaction under typical conditions is kinetically controlled [67, 68]. As a consequence, we decided to try to find some parameters and/or rules for predicting the regioselectivity of BH additions on IPR EMFs under kinetic control.

To that end, we computationally studied the Bingel-Hirsch addition of diethylbromomalonate over all 13 nonequivalent bonds of $\text{Sc}_3\text{N}@D_{3h}\text{-C}_{78}$ EMF at BP86-D2/TZP//BP86-D2/DZP level [69]. In Figure 10 we summarize the results obtained. Our computations revealed that the addition to bond **6** has the lowest activation energy among all possible additions (barrier of 7.3 kcal/mol). This result is in agreement with the experimental monoadduct detected and characterized by means of NMR measures by Dorn and co-workers [70]. In addition, we found that those bonds presenting the most exothermic reaction energies do not coincide with those having the lowest reaction barriers, as previously reported for BH additions on non-IPR EMFs [67, 68].

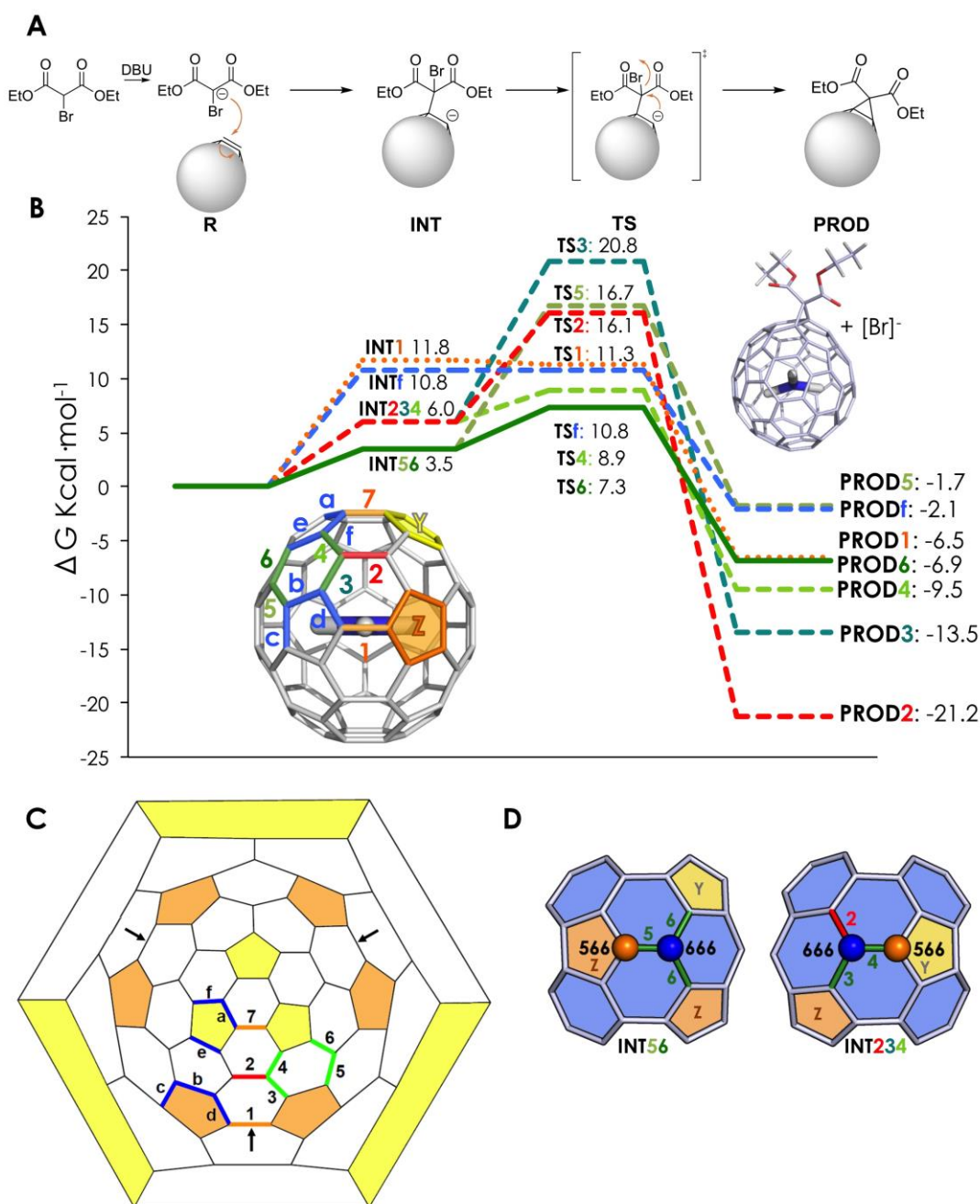


Figure 10. A) The Bingel-Hirsch mechanism. B) Gibbs energy profile for the BH cycloaddition to selected non-equivalent bonds of $\text{Sc}_3\text{N}@D_{3h}\text{-C}_{78}$ (in kcal/mol). C) Representation of the seven non-equivalent [6,6] bonds: pyracylene bonds **1** and **7**, pyrene or type C bond **2**, and type B bonds **3**, **4**, **5**, and **6**; and the six types of [5,6] D corannulene bonds, **a-f**. D) Schematic representation of intermediates **int56** and **int234**. Blue carbon atoms (in spheres) represent the initial addition site corresponding to *int666*; orange carbon atoms denote *int566*. For clarity, 6-MRs are colored in blue, Z-5-MRs in orange and Y-5-MRs in light yellow. Reprinted with permission from ref. [69].

The lowest energy intermediate **int56**, which leads to the kinetic product **6** formation, and **int234** are substantially lower in energy than the other possible intermediates (see Figure 10). We have found that the aromaticity can be used to understand why those intermediates corresponding to the attack on a carbon atom situated in a three hexagonal rings junction (denoted as *int666* in Figure 10) are the most stable ones. First, 5-MRs in EMFs are those that concentrate the negative charge transferred from the metal to the fullerene structure, thus

become more aromatic. Then, *int666* intermediates are more stable than *int566* because in the former no 5-MRs aromaticity is lost in the attack to the C atom. And second, the formed intermediate is negatively charged, with the negative charge delocalized on the vicinity of the attacked carbon atom. Therefore, those intermediates having 5-MRs on neighbor positions, as *int56* and *int234*, will be able to better stabilize the extra negative charge (see Figure 10D).

The difference in the reaction activation barrier for the formation of products **5** and **6** (*ca.* 10 kcal/mol), which come from the same intermediate (see Figure 10), has also been rationalized in terms of aromaticity measures. Because of the proximity of the metal atoms, 5-MRs **Z** in $\text{Sc}_3\text{N}@D_{3h}\text{-C}_{78}$ are more aromatic than **Y** 5-MRs. It is energetically more favored to attack the less aromatic **Y** 5-MR than **Z** 5-MRs during the nucleophilic attack in the second step of the BH reaction (Figure 10A). In general, our calculations indicate that the cyclopropane ring closure is preferred to be on 5-MRs than 6-MRs because 5-MRs are better nucleophiles. In addition to that, we observed that closed-cage products are usually obtained when the cyclopropane ring closure takes place on a carbon atom having a lower pyramidalization angle and located in a ring with low aromatic character. On the other hand, open-cage products usually present a high pyramidalization angle of the attacked carbon atom located in a ring with large aromatic character.

The understanding of the BH reactivity patterns observed in the case of $\text{Sc}_3\text{N}@D_{3h}\text{-C}_{78}$ in terms of aromaticity we proposed an aromaticity-based criteria (Predictive Aromaticity Criteria, PAC) to predict the regioselectivity of Bingel-Hirsch additions on IPR EMFs (see Figure 11) [69].

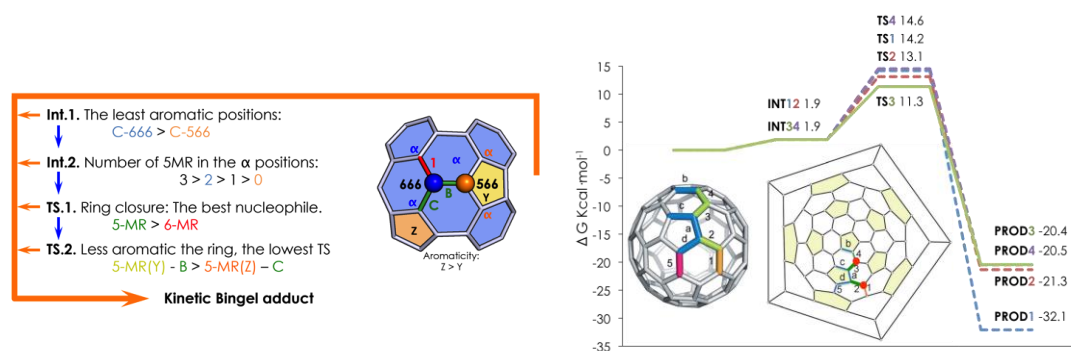


Figure 11. Left: Predictive Aromaticity-based rules for the Bingel-Hirsch addition on IPR EMFs; Right: Gibbs energy profile for the BH cycloaddition to selected non-equivalent bonds of $\text{Sc}_3\text{N}@D_{5h}\text{-C}_{80}$ (in kcal/mol) and the representation of the five non-equivalent [6,6] bonds: pyrene bond type bond **1**, pyracylene bond **5**, and type B bonds **2**, **3**, **4**, and **5**; and the four type D corannulene bonds **a-d**. Adapted from ref. [69].

We subsequently applied the PAC criteria to predict the regioselectivity of BH addition on the challenging $\text{Sc}_3\text{N}@D_{5h}\text{-C}_{80}$ system. The $D_{5h}\text{-C}_{80}$ cage has 9 different possible addition sites (see Figure 11), and the TNT cluster can freely rotate inside. Applying our proposed aromaticity criteria, we identified two possible *int666* on the $\text{Sc}_3\text{N}@D_{5h}\text{-C}_{80}$ EMF, *int12* and *int34* as shown in Figure 11, and predicted *int34* to be slightly more stable because of having 3 pentagons on vicinity positions. According to PAC, and our aromaticity calculations, which indicate that 5-MR rings containing bonds **a-c-d** are less aromatic than 5-MR rings containing bond **b**, we concluded that the formation of product **3** should be more favored.

The computational exploration of the BH reaction on all 9 different addition sites, considering 7 different orientations of the inner cluster, is in complete agreement with the PAC prediction. The Gibbs energy profiles for some selected additions are shown in Figure 11. As predicted, intermediates *int12* and *int34* are those more stable, and the transition state for the formation

of product **3** is the one lowest in energy, thus being the proposed kinetic product for the BH addition on Sc₃N@D_{5h}-C₈₀ EMF.

The PAC predictions for the BH addition on Sc₃N@D_{5h}-C₈₀ EMF were also experimentally tested [69]. Three different monoadducts were obtained, the major isomer being the one corresponding to product **3** as predicted initially by the PAC criteria, and our subsequent computational exploration. The excellent agreement between our proposed PAC predictions and the experiments indicates that these rules are rather general and could be extensible to other IPR EMFs.

Conclusions

It is generally considered that aromaticity does not play a fundamental role in determining the molecular structure and reactivity of neutral and hollow fullerenes. However, the situation is the opposite when we consider charged fullerenes [71]. In reduced fullerenes or fullerenes with encapsulated metal clusters (endohedral metallofullerenes, EMFs), aromaticity plays a relevant role that has not been taken into account when discussing the structure and reactivity of EMFs until recently. In this review, we emphasize the role that aromaticity plays in EMFs and negatively charged fullerenes by analyzing five different situations, namely, the regioselectivity of Diels-Alder reactions in reduced C₆₀, the choice of the most suitable hosting cages in EMFs, the stability of EMF adducts formed in Bingel-Hirsch (BH) reactions, and the existence of structural criteria to predict the regioselectivity in BH reactions. It is likely that coming works will further reinforce the importance of aromaticity in endohedral metallofullerene chemistry.

Acknowledgements

We are grateful for financial support from the Spanish MINECO (CTQ2014-54306-P, CTQ2014-52525-P, CTQ2014-59212-P, and RyC contract to S.O.), the Catalan DIUE (2014SGR931, ICREA Academia 2014 Award to M.S. and XRQTC), and the FEDER fund (UNGI10-4E-801). M.G.-B. thanks the Spanish MECO for a PhD grant (AP2010-2517) and the Ramón Areces Foundation for a postdoctoral fellowship. S.O. thanks the European Community for CIG project (PCIG14-GA-2013-630978), and the funding from the European Research Council (ERC) under the European Union's Horizon 2020 research and innovation program (ERC-2015-StG-679001). CSUC and BSC-CNS are acknowledged. Last but not least we thank Prof. Luis Echegoyen for his continuous support and collaboration.

References

- [1] H.W. Kroto, J.R. Heath, S.C. O'Brien, R.F. Curl, R.E. Smalley, C₆₀ - Buckminsterfullerene, *Nature*, 318 (1985) 162-163.
- [2] S. Iijima, Direct observation of the tetrahedral bonding in graphitized carbon black by high resolution electron microscopy, *J. Cryst. Growth*, 50 (1980) 675-683.
- [3] S. Iijima, The 60-carbon cluster has been revealed, *J. Phys. Chem.*, 91 (1987) 3466-3467.
- [4] J.M. Hawkins, A. Meyer, T.A. Lewis, S. Loren, F.J. Hollander, Crystal structure of osmylated C₆₀: confirmation of the soccer ball framework, *Science*, 252 (1991) 312-313.
- [5] M. Bühl, A. Hirsch, Spherical aromaticity of fullerenes, *Chem. Rev.*, 101 (2001) 1153-1183.
- [6] H.W. Kroto, A.W. Allaf, S.P. Balm, C₆₀: Buckminsterfullerene, *Chem. Rev.*, 91 (1991) 1213-1235.
- [7] N. Martín, L. Sánchez, B. Illescas, I. Pérez, C₆₀-Based Electroactive Organofullerenes, *Chem. Rev.*, 98 (1998) 2527-2548.

- [8] C. Thilgen, F. Diederich, Structural Aspects of Fullerene Chemistry. A Journey through Fullerene Chirality, *Chem. Rev.*, 106 (2006) 5049-5135.
- [9] M.D. Tzirakis, M. Orfanopoulos, Radical Reactions of Fullerenes: From Synthetic Organic Chemistry to Materials Science and Biology, *Chem. Rev.*, 113 (2013) 5262-5321.
- [10] J.L. Delgado, N. Martin, P. de la Cruz, F. Langa, Pyrazolinofullerenes: a less known type of highly versatile fullerene derivatives, *Chem. Soc. Rev.*, 40 (2011) 5232-5241.
- [11] D.M. Guldi, Fullerene-porphyrin architectures; photosynthetic antenna and reaction center models, *Chem. Soc. Rev.*, 31 (2002) 22-36.
- [12] D.M. Guldi, B.M. Illescas, C.M. Atienza, M. Wielopolski, N. Martin, Fullerene for organic electronics, *Chem. Soc. Rev.*, 38 (2009) 1587-1597.
- [13] J.L. Segura, N. Martin, [60]Fullerene dimers, *Chem. Soc. Rev.*, 29 (2000) 13-25.
- [14] Y. Zhang, K.B. Ghiassi, Q. Deng, N.A. Samoylova, M.M. Olmstead, A.L. Balch, A.A. Popov, Synthesis and Structure of $\text{LaSc}_2\text{N}@C_s(\text{hept})-C_{80}$ with One Heptagon and Thirteen Pentagons, *Angew. Chem. Int. Ed.*, 54 (2015) 495-499.
- [15] W. Qian, S.-C. Chuang, R.B. Amador, T. Jarrosson, M. Sander, S. Pieniazek, S.I. Khan, Y. Rubin, Synthesis of Stable Derivatives of C_{62} : The First Nonclassical Fullerene Incorporating a Four-Membered Ring, *J. Am. Chem. Soc.*, 125 (2003) 2066-2067.
- [16] H.W. Kroto, The stability of the fullerenes C_n , with $n = 24, 28, 32, 36, 50, 60$ and 70 , *Nature*, 329 (1987) 529 - 531.
- [17] J.R. Heath, S.C. Obrien, Q. Zhang, Y. Liu, R.F. Curl, H.W. Kroto, F.K. Tittel, R.E. Smalley, Lanthanum complexes of spheroidal carbon shells, *J. Am. Chem. Soc.*, 107 (1985) 7779-7780.
- [18] Y. Chai, T. Guo, C. Jin, R.E. Haufler, L.P.F. Chibante, J. Fure, L. Wang, J.M. Alford, R.E. Smalley, Fullerenes with metals inside, *J. Phys. Chem.*, 95 (1991) 7564-7568.
- [19] M. Takata, B. Umeda, E. Nishibori, M. Sakata, Y. Saito, M. Ohno, H. Shinohara, Confirmation by X-ray diffraction of the endohedral nature of the metallofullerene $Y@C_{82}$, *Nature*, 377 (1995) 46-49.
- [20] M.N. Chaur, F. Melin, A.L. Ortiz, L. Echegoyen, Chemical, Electrochemical, and Structural Properties of Endohedral Metallofullerenes, *Angew. Chem. Int. Ed.*, 48 (2009) 7514-7538.
- [21] X. Lu, T. Akasaka, S. Nagase, Rare Earth Coordination Chemistry: Fundamentals and Applications, Wiley-Blackwell, Singapore, 2009.
- [22] S. Stevenson, G. Rice, T. Glass, K. Harich, F. Cromer, M.R. Jordan, J. Craft, E. Hadju, R. Bible, M.M. Olmstead, K. Maitra, A.J. Fisher, A.L. Balch, H.C. Dorn, Small-bandgap endohedral metallofullerenes in high yield and purity, *Nature*, 401 (1999) 55-57.
- [23] A.A. Popov, L. Dunsch, Bonding in Endohedral Metallofullerenes as Studied by Quantum Theory of Atoms in Molecules, *Chem. Eur. J.*, 15 (2009) 9707-9729.
- [24] Z.-Q. Shi, X. Wu, C.-R. Wang, X. Lu, H. Shinohara, Isolation and Characterization of $\text{Sc}_2\text{C}_2@C_{68}$: A Metal-Carbide Endofullerene with a Non-IPR Carbon Cage, *Angew. Chem. Int. Ed.*, 45 (2006) 2107-2111.
- [25] J.M. Campanera, C. Bo, J.M. Poblet, General rule for the stabilization of fullerene cages encapsulating trimetallic nitride templates, *Angew. Chem. Int. Ed.*, 44 (2005) 7230-7233.
- [26] R. Valencia, A. Rodríguez-Forteza, J.M. Poblet, Large fullerenes stabilized by encapsulation of metallic clusters, *Chem. Commun.*, (2007) 4161-4163.
- [27] A. Rodríguez-Forteza, A.L. Balch, J.M. Poblet, Endohedral metallofullerenes: a unique host-guest association, *Chem. Soc. Rev.*, 40 (2011) 3551-3563.
- [28] A.A. Popov, L. Dunsch, Structure, Stability, and Cluster-Cage Interactions in Nitride Clusterfullerenes $M_3N@C_{2n}$ ($M = \text{Sc}, \text{Y}; 2n = 68-98$): a Density Functional Theory Study, *J. Am. Chem. Soc.*, 129 (2007) 11835-11849.
- [29] A. Rodríguez-Forteza, N. Alegret, A.L. Balch, J.M. Poblet, The maximum pentagon separation rule provides a guideline for the structures of endohedral metallofullerenes, *Nat. Chem.*, 2 (2010) 955-961.
- [30] H. Zettergren, M. Alcami, F. Martín, Stable Non-IPR C_{60} and C_{70} Fullerenes Containing a Uniform Distribution of Pyrenes and Adjacent Pentagons, *ChemPhysChem*, 9 (2008) 861-866.

- [31] M. Garcia-Borràs, S. Osuna, M. Swart, J.M. Luis, M. Solà, Maximum Aromaticity as a Guiding Principle for the Most Suitable Hosting Cages in Endohedral Metallofullerenes, *Angew. Chem. Int. Ed.*, 52 (2013) 9275-9278.
- [32] M. Garcia-Borràs, S. Osuna, J.M. Luis, M. Solà, Rationalizing the relative abundances of trimetallic nitride template-based endohedral metallofullerenes from aromaticity measures, *Chem. Commun.*, 53 (2017) 4140-4143.
- [33] M. Garcia-Borràs, S. Osuna, J.M. Luis, M. Swart, M. Solà, The Exohedral Diels–Alder Reactivity of the Titanium Carbide Endohedral Metallofullerene $\text{Ti}_2\text{C}_2@D_{3h}\text{-C}_{78}$: Comparison with $D_{3h}\text{-C}_{78}$ and $M_3N@D_{3h}\text{-C}_{78}$ (M=Sc and Y) Reactivity, *Chem. Eur. J.*, 18 (2012) 7141-7154.
- [34] S. Osuna, M. Swart, M. Solà, The reactivity of endohedral fullerenes. What can be learnt from computational studies?, *Phys. Chem. Chem. Phys.*, 13 (2011) 3585-3603.
- [35] M. Bühl, The relation between endohedral chemical shifts and local aromaticities in fullerenes, *Chem. Eur. J.*, 4 (1998) 734-739.
- [36] M. Garcia-Borràs, S. Osuna, M. Swart, J.M. Luis, L. Echegoyen, M. Solà, Aromaticity as the driving force for the stability of non-IPR endohedral metallofullerene Bingel-Hirsch adducts, *Chem. Commun.*, 49 (2013) 8767-8769.
- [37] S. Osuna, R. Valencia, A. Rodríguez-Forteza, M. Swart, M. Solà, J.M. Poblet, Full Exploration of the Diels–Alder Cycloaddition on Metallofullerenes $M_3N@C_{80}$ (M=Sc, Lu, Gd): The D_{5h} versus I_h Isomer and the Influence of the Metal Cluster, *Chem. Eur. J.*, 18 (2012) 8944-8956.
- [38] P.P. Fatouros, F.D. Corwin, Z.J. Chen, W.C. Broaddus, J.L. Tatum, B. Kettenmann, Z. Ge, H.W. Gibson, J.L. Russ, A.P. Leonard, J.C. Duchamp, H.C. Dorn, In vitro and in vivo imaging studies of a new endohedral metallofullerene nanoparticle, *Radiology*, 240 (2006) 756-764.
- [39] X. Lu, L. Feng, T. Akasaka, S. Nagase, Current status and future developments of endohedral metallofullerenes, *Chem. Soc. Rev.*, 41 (2012) 7723-7760.
- [40] A.A. Popov, S. Yang, L. Dunsch, Endohedral Fullerenes, *Chem. Rev.*, 113 (2013) 5989-6113.
- [41] E.B. Iezzi, J.C. Duchamp, K. Harich, T.E. Glass, H.M. Lee, M.M. Olmstead, A.L. Balch, H.C. Dorn, A symmetric derivative of the trimetallic nitride endohedral metallofullerene, $\text{Sc}_3\text{N}@C_{80}$, *J. Am. Chem. Soc.*, 124 (2002) 524-525.
- [42] J.M. Campanera, C. Bo, J.M. Poblet, Exohedral Reactivity of Trimetallic Nitride Template (TNT) Endohedral Metallofullerenes, *J. Org. Chem.*, 71 (2005) 46-54.
- [43] M. Garcia-Borràs, S. Osuna, J.M. Luis, M. Swart, M. Solà, A Complete Guide on the Influence of Metal Clusters in the Diels–Alder Regioselectivity of $I_h\text{-C}_{80}$ Endohedral Metallofullerenes, *Chem. Eur. J.*, 19 (2013) 14931-14940.
- [44] C.M. Cardona, B. Elliott, L. Echegoyen, Unexpected chemical and electrochemical properties of $M_3N@C_{80}$ (M = Sc, Y, Er), *J. Am. Chem. Soc.*, 128 (2006) 6480-6485.
- [45] A. Rodríguez-Forteza, J.M. Campanera, C.M. Cardona, L. Echegoyen, J.M. Poblet, Dancing on a fullerene surface: Isomerization of $Y_3N@(N\text{-ethylpyrrolidino-}C_{80})$ from the 6,6 to the 5,6 regioisomer, *Angew. Chem. Int. Ed.*, 45 (2006) 8176-8180.
- [46] M.R. Cerón, M. Izquierdo, M. Garcia-Borràs, S.S. Lee, S. Stevenson, S. Osuna, L. Echegoyen, Bis-1,3-dipolar Cycloadditions on Endohedral Fullerenes $M_3N@I_h\text{-C}_{80}$ (M = Sc, Lu): Remarkable Endohedral-Cluster Regiochemical Control, *J. Am. Chem. Soc.*, 137 (2015) 11775-11782.
- [47] T. Cai, C. Slebodnick, L. Xu, K. Harich, T.E. Glass, C. Chancellor, J.C. Fettinger, M.M. Olmstead, A.L. Balch, H.W. Gibson, H.C. Dorn, A pirouette on a metallofullerene sphere: Interconversion of isomers of N-tritylpyrrolidino I_h $\text{Sc}_3\text{N}@C_{80}$, *J. Am. Chem. Soc.*, 128 (2006) 6486-6492.
- [48] S. Aroua, M. Garcia-Borràs, S. Osuna, Y. Yamakoshi, Essential Factors for Control of the Equilibrium in the Reversible Rearrangement of $M_3N@I_h\text{-C}_{80}$ Fulleropyrrolidines: Exohedral Functional Groups versus Endohedral Metal Clusters, *Chem. Eur. J.*, 20 (2014) 14032-14039.

- [49] O. Lukoyanova, C.M. Cardona, J. Rivera, L.Z. Lugo-Morales, C.J. Chancellor, M.M. Olmstead, A. Rodríguez-Fortea, J.M. Poblet, A.L. Balch, L. Echegoyen, "Open rather than closed" malonate methano-fullerene derivatives. The formation of methanofulleroid adducts of $Y_3N@C_{80}$, *J. Am. Chem. Soc.*, 129 (2007) 10423-10430.
- [50] S. Osuna, A. Rodríguez-Fortea, J.M. Poblet, M. Solà, M. Swart, Product formation in the Prato reaction on $Sc_3N@D_{5h}-C_{80}$: preference for [5,6]-bonds, and not pyracylenic bonds, *Chem. Commun.*, 48 (2012) 2486.
- [51] S. Osuna, M. Swart, J.M. Campanera, J.M. Poblet, M. Solà, Chemical reactivity of $D_{3h} C_{78}$ (Metallo)fullerene: Regioselectivity changes induced by Sc_3N encapsulation, *J. Am. Chem. Soc.*, 130 (2008) 6206-6214.
- [52] S. Osuna, M. Swart, M. Solà, The Diels-Alder Reaction on Endohedral $Y_3N@C_{78}$: The Importance of the Fullerene Strain Energy, *J. Am. Chem. Soc.*, 131 (2009) 129-139.
- [53] F.M. Bickelhaupt, M. Solà, I. Fernández, Understanding the Reactivity of Endohedral Metallofullerenes: C_{78} versus $Sc_3N@C_{78}$, *Chem. Eur. J.*, 21 (2015) 5760-5768.
- [54] M. Solà, J. Mestres, J. Martí, M. Duran, An AM1 Study of the Reactivity of Buckminsterfullerene (C_{60}) in a Diels-Alder Model Reaction, *Chem. Phys. Lett.*, 231 (1994) 325-330.
- [55] I. Fernández, M. Solà, F.M. Bickelhaupt, Why Do Cycloaddition Reactions Involving C_{60} Prefer [6,6] over [5,6] Bonds?, *Chem. Eur. J.*, 19 (2013) 7416-7422.
- [56] M. Garcia-Borràs, S. Osuna, M. Swart, J.M. Luis, M. Solà, Electrochemical control of the regioselectivity in the exohedral functionalization of C_{60} : the role of aromaticity, *Chem. Commun.*, 49 (2013) 1220-1222.
- [57] P. Salvador, E. Ramos-Cordoba, APOST-3D, Institute of Computational Chemistry, Universitat de Girona, Girona, 2011.
- [58] E. Matito, M. Solà, P. Salvador, M. Duran, Electron sharing indexes at the correlated level. Application to aromaticity calculations, *Faraday discussions*, 135 (2007) 325-345.
- [59] E. Matito, M. Duran, M. Sola, The aromatic fluctuation index (FLU): A new aromaticity index based on electron delocalization, *J. Chem. Phys.*, 122 (2005) 014109; Erratum *ibid* 125 (2006) 059901.
- [60] E. Matito, ESI-3D: Electron sharing indexes program for 3D molecular space partitioning, Institute of Computational Chemistry, Girona, 2006.
- [61] J. Cioslowski, E. Matito, M. Sola, Properties of aromaticity indices based on the one-electron density matrix, *J. Phys. Chem. A*, 111 (2007) 6521-6525.
- [62] T.M. Krygowski, Crystallographic studies of Inter- and Intra-Molecular Interactions Reflected in benzenoid Hydrocarbons. Nonequivalence of Indices of Aromaticity, *J. Chem. Inf. Comp. Sci.*, 33 (1993) 70-78.
- [63] J. Kruszewski, T.M. Krygowski, Definition of aromaticity basing on the harmonic oscillator model, *Tetrahedron Lett.*, 13 (1972) 3839-3842.
- [64] Z. Badri, C. Foroutan-Nejad, Unification of ground-state aromaticity criteria - structure, electron delocalization, and energy - in light of the quantum chemical topology, *Physical Chemistry Chemical Physics*, 18 (2016) 11693-11699.
- [65] E. Albertazzi, C. Domene, P. W. Fowler, T. Heine, G. Seifert, C. Van Alsenoy, F. Zerbetto, Pentagon adjacency as a determinant of fullerene stability, *Phys. Chem. Chem. Phys.*, 1 (1999) 2913-2918.
- [66] M.R. Cerón, F.-F. Li, L. Echegoyen, An Efficient Method to Separate $Sc_3N@C_{80} I_h$ and D_{5h} Isomers and $Sc_3N@C_{78}$ by Selective Oxidation with Acetylferrocenium $[Fe(COCH_3C_5H_4)Cp]^+$, *Chem. Eur. J.*, 19 (2013) 7410-7415.
- [67] N. Alegret, A. Rodríguez-Fortea, J.M. Poblet, Bingel-Hirsch Addition on Endohedral Metallofullerenes: Kinetic Versus Thermodynamic Control, *Chem. Eur. J.*, 19 (2013) 5061-5069.
- [68] N. Alegret, P. Salvadó, A. Rodríguez-Fortea, J.M. Poblet, Bingel-Hirsch Addition on Non-Isolated-Pentagon-Rule $Gd_3N@C_{2n}$ ($2n = 82$ and 84) Metallofullerenes: Products under Kinetic Control, *J. Org. Chem.*, 78 (2013) 9986-9990.

- [69] M. Garcia-Borràs, M.R. Cerón, S. Osuna, M. Izquierdo, J.M. Luis, L. Echegoyen, M. Solà, The Regioselectivity of Bingel–Hirsch Cycloadditions on Isolated Pentagon Rule Endohedral Metallofullerenes, *Angew. Chem. Int. Ed.*, 55 (2016) 2374-2377.
- [70] T. Cai, L. Xu, C. Shu, H.A. Champion, J.E. Reid, C. Anklin, M.R. Anderson, H.W. Gibson, H.C. Dorn, Selective Formation of a Symmetric $\text{Sc}_3\text{N}@C_{78}$ Bisadduct: Adduct Docking Controlled by an Internal Trimetallic Nitride Cluster, *J. Am. Chem. Soc.*, 130 (2008) 2136-2137.
- [71] M. Garcia-Borràs, S. Osuna, J.M. Luis, M. Swart, M. Solà, The role of aromaticity in determining the molecular structure and reactivity of (endohedral metallo)fullerenes, *Chem. Soc. Rev.*, 43 (2014) 5089-5105.